Preparation of *Stellera chamaejasme* L. Mesoporous Activated Carbon by Rubidium Chloride Chemical Method

Shimin Dang, Jianxia Guo, Ze Liu, and Haichao Li *

To make use of rubidium salt resources in the Qinghai Salt Lake and to valorize *Stellera chamaejasme* L., mesoporous activated carbon was prepared by a chemical activation method using rubidium chloride as an activator. Using methylene blue and iodine as pollutant models, the adsorption capacity of mesoporous activated carbon was determined. The specific surface area, pore structure, and surface functional groups of mesoporous activated carbon were determined using a fully automated specific surface area analyzer, X-ray diffractometer (XRD), Raman spectrometer, scanning electron microscope (SEM), Fourier transform infrared spectrometer (FT- IR), and an X-ray electron spectrometer (XPS). The surface functional groups of mesoporous activated carbon were found to be mainly comprised of carbon and oxygen. The mesoporous activated carbon had a certain graphitized microcrystalline structure. The carbon yield of the mesoporous activated carbon was 13.55% ± 0.41%, the specific surface area was 877.02 m^2/g, the adsorption amount of iodine, 891.35 mg/g, and the adsorption amount of methylene blue, 256.95 mg/g. The dominant pore size was 0.945 nm, the average pore size was 2.43 nm, and the pore volume was 0.26 cm^3/g.

DOI: 10.15376/biores.19.4.8312-8323

Keywords: Stellera chamaejasme L.; Rubidium chloride; Mesoporous activated carbon

*Contact information: Qinghai Nationalities University, Key Laboratory of Applied Physical Chemistry of Qinghai Province, Qinghai810007, China; *Corresponding author: lihaichao@vip.163.com*

INTRODUCTION

A poisonous plant known as *Stellera chamaejasme* L. grows on the Tibetan Plateau in China (Li *et al.* 2009). *Stellera chamaejasme,* also known as broken intestines, steamed bread flowers, and mountain radish, has excellent resistance to drought and tenacious vitality in the Tibetan Plateau. It exhibits rapid growth as it continues to take over the local plant space, poisoning livestock and poultry. The spread of *S. chamaejasme* is a sign of local ecological degradation. It has been reported that *S. chamaejasme* is mainly used in the medical and paper industries (Li *et al.* 2009; Jo *et al.* 2020). To reduce the burden on the ecosystem and increase the utilization rate of *S. chamaejasme*, a targeted expansion of the fields of application of *Stellera chamaejasme* is needed.

Activated carbon is a general term for carbon materials with high specific surface area and strong adsorption capacity (Zhang *et al.* 2022). Activated carbon has a wide range of applications and is often used in medical, industrial production, food hygiene and other industries (Zhang *et al.* 2023). Chen *et al.* (2015) prepared activated carbon from *S. chamaejasme* by a chemical activation method. The quality of the *S. chamaejasme* is mainly concentrated in its root, which is structured by the epidermis, endodermis, and

mesostyle. The root material mainly consists of dry matter, benzyl alcohol extract, cellulose, and other elements. From the carbon content of the elements contained in its roots, *S. chamaejasme* is a good raw material for the preparation of activated carbon (Zhao *et al.* 2023).

The dissolved content of Qinghai Salt Lake is a lake dominated by chloride salts, with a variety of salt minerals co-existing (Du 2014). The salt substances in Qinghai salt lake are mainly potassium salt and lithium salt. The proven lithium reserves in the salt lake reach 17.24 million tons (Chen *et al.* 2024). Qinghai Salt Lake contains rubidium and caesium resources that are scarce in the outside world. Using rubidium chloride as activator and lignin as raw material, Zhang (2024) successfully prepared a carbon adsorption material with a specific surface area of 433 m^2/g under the activation temperature of 600 ℃. The study shows that rubidium chloride can be used as an activator.

In this study, the activated carbon of *S. chamaejasme* was prepared using salt lake rubidium chloride as an activator. This experiment provides fundamental research data for the protection of Qinghai's environment, exploitation of salt lake resources, and subsequent research on the activation mechanism of chlor-alkali metals.

MATERIALS AND METHODS

Materials

Stellera chamaejasme (secondary treatment required) was picked from the Huangyuan Grassland in Qinghai. Rubidium chloride (AR, 99.9%), calcium hydroxide (AR, 99.9%), Iodine solution (1.2 g/L), and Methylene blue solution (400 mg/L) were purchased from Aladdin. The drugs were used directly without post-treatment, and the water used in the experiments was deionized water.

Preparation of Activated Carbons

The *S. chamaejasme* root was peeled. The middle layer of white bast was cleaned and added to the calcium hydroxide for cooking to extract crude fiber (cooking time 2 h, temperature 60 °C). The crude fiber was washed until the washing solution became neutral, and then the course fibers were repeatedly pounded into pulp. The pulp water was sieved and filtered, and the filtered product was placed in a cool place to dry.

According to the preset impregnation ratio (raw material: activator), the treated *S. chamaejasme* and rubidium chloride were weighed, with the mass of the pretreated *S. chamaejasme* always being 10 g. The next step was to add 30 mL of deionized water and mix the raw materials with the activator. The oven temperature was set to 70 °C and the mixture was dried for 40 minutes to remove excess moisture. The muffle furnace temperature was set to 700 °C, the heating rate to 10 °C/min, the holding time to 120 min, and calcination of the mixture was performed. This was followed by washing the calcined product with deionized water to neutrality, drying, and grinding to obtain activated carbon.

Characterization Methods

Carbon yield and ash content are important indicators used to judge the yield of activated carbon and raw material selection. The charcoal yield was calculated from the ratio of the mass of activated charcoal to the mass of the raw material. A blank control experiment was set up to calculate the ash content using the difference in mass before and after the raw material (Kim *et al.* 2023). The prefabricated waterproofing ratio was set to

1:3, 1:2, 1:1, 2:1, 3:1, 5:1, and 10:1. (Zhang *et al.* 2024; Chen *et al.* 2015).

The adsorption capacity of activated carbon for methylene blue was determined by the requirements of GB/T12496.10-2015. The specific operational steps were: mixing the sample with the configured methylene blue solution, determining the transmittance of light of the mixed solution with a spectrophotometer, and when the transmittance of light met the requirements, the number of milliliters of methylene blue solution titrated at this transmittance was the adsorption volume of activated carbon on methylene blue. The iodine value adsorption was determined with reference to GB/T12496.8-2015, and the determination process was the same as methylene blue (Ahmed *et al.* 2014; Ren *et al.* 2024).

The N_2 adsorption-desorption experiments were carried out on the activated carbon using a TriStarI 3020 fully automated specific surface area and pore analyzer (Micromeritics, USA) at 77 k. The pore size and specific surface area size of the activated carbon were determined based on the N_2 adsorption-desorption measurements (Doczekalska *et al.* 2022).

The activated carbon was gold-sprayed in a vacuum coater. The acquisition time was set at 100 s, the intensification voltage was 20 KV, the scanning spacing was 15 mm, and the surface of the activated carbon was photographed using a SU8010 field emission scanning electron microscope (Hitachi, Japan) (Columba *et al.* 2022).

The microcrystalline structure of the activated carbon was scanned using a D/MaX-2550PC X-ray diffractometer (RIGAKU, Japan) within a diffraction angle range of 2θ = 10 to 70° and a diffraction rate of 4°/min. The graphitized degree of activated carbon was determined using NEXUS-670 FTIR-Raman spectrometer (Nicolet, USA) at an excitation wavelength of 530 nm (Kunusa *et al.* 2021).

A Nicolet™ is50 Fourier transform infrared spectrometer (PerkinElmer, USA) was used to test the absorbance peaks of the functional groups on the surface of the activated carbon using the spectrometer by setting the scanning wavelength of the instrument to 400 to 4000 cm^{-1}. The pressure of the analysis chamber was set at 3×10^{-10} mbar and the incident wavelength of X-rays was 500 μm, and the elements contained on the surface of the activated carbon were analyzed by using an ESCLAB Xi X-ray photoelectron spectrometer (Shenzhen Core Derun Electronic Technology Co Ltd.) (Wang *et al.* 2017).

All test methods were carried out three times for each condition.

RESULTS AND DISCUSSION

Characterization of Activated Carbon

High ash content affects the formation of pores on the surface of activated carbon (Kim *et al.* 2023). Ash content is one of the most important indicators of whether a substance can be used as a raw material for the preparation of activated carbon. The ash mass percentage of pretreated *S. chamaejasme* was 3.12% ± 0.15% as measured relative to a blank experiment. In terms of ash content, *S. chamaejasme* is similar to common raw materials for activated carbon processing, such as coconut shells and straw, and is a low ash content raw material (Buah *et al.* 2019). Figure 1 shows the graph of activated carbon yield *versus* impregnation ratio under the experimental conditions of activation temperature of 700 °C and activation time of 2 h. The activated charcoal yield was found to increase with the increase of the impregnation ratio; when the impregnation ratio is 1:1, the charcoal yield reaches a peak of 13.55% ± 0.41%.

Zhang *et al.* (2023) prepared activated carbon with a carbon yield of 7.42% using cellulose as the raw material and cesium chloride as the activator. Chen *et al.* (2015) used *S. chamaejasme* as the raw material and phosphoric acid as the activator to prepare activated carbon with a high carbon yield of 57.41%. By comparing the carbon yield, the carbon yield of the activated carbon produced in this study was classed as moderate.

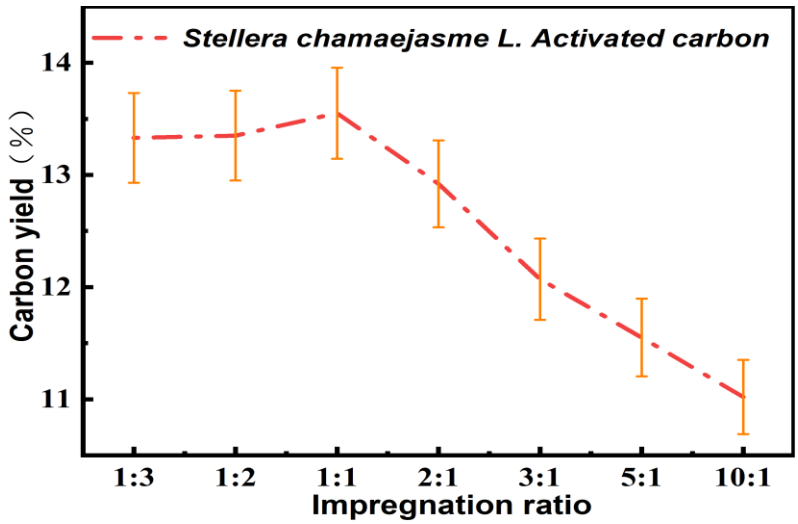

Fig. 1. Activated carbon yield as a function of impregnation ratio (*S. chamaejasme*: Rubidium chloride)

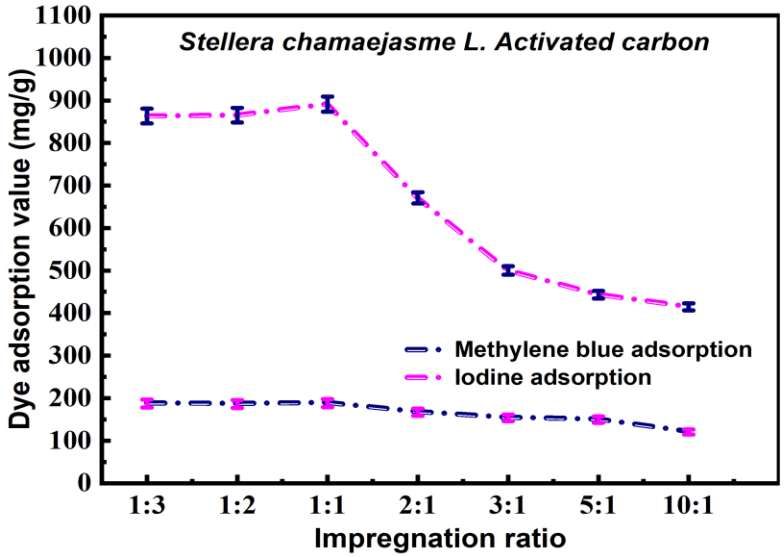

Fig. 2. Adsorption of activated carbon dyes as a function of the impregnation ratio (*S. chamaejasme*: Rubidium chloride)

Methylene blue and iodine were taken as pollutant models, and the adsorption capacity of activated carbon was determined by observing the adsorption value of activated carbon to pollutants. Figure 2 shows the dye adsorption on activated carbon prepared with different impregnation ratios under the experimental conditions of activation temperature of 700 °C and activation time of 2 h.

As can be seen from Fig. 2, the non-activated *S. chamaejasme* did not have the ability to adsorb significant amounts of methylene blue and iodine. After activation, the adsorption capacity of *S. chamaejasme* toward iodine and methylene blue increased greatly, and the adsorption capacity of *S. chamaejasme* activated carbon toward dye increased with decreasing impregnation ratio. The adsorption value of activated charcoal for dyes reached a peak value when the impregnation ratio was 1:1. The adsorption capacity for iodine was 891 mg/g, and for methylene blue it was 257 mg/g.

Specific surface area and pore structure data of activated carbon are important indicators to judge the adsorption performance of activated carbon. The specific surface area and pore size of activated carbon can be determined by the adsorption-desorption test with nitrogen. Figure 3 shows the specific surface area of activated carbon versus the impregnation ratio, from which the specific surface area of activated carbon will increase with the impregnation ratio, first reaching a peak and then decreasing. The maximum value of the specific surface area of activated carbon was obtained at the impregnation ratio of 1:1, and the maximum specific surface area was 877 m^2/g.

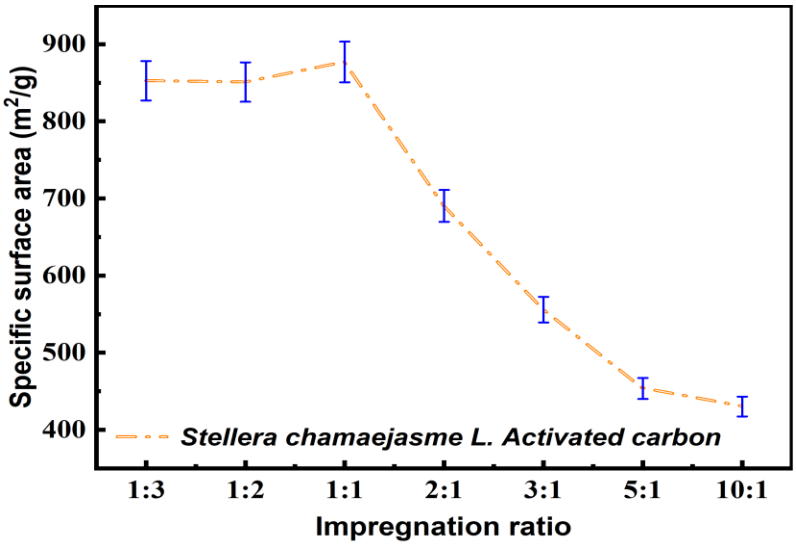

Fig. 3. Plot of activated carbon impregnation ratio versus specific surface area (*S. chamaejasme*: Rubidium chloride)

A comprehensive analysis of the carbon yield, dye adsorption capacity of activated carbon, and specific surface area showed that the best performance of the activated carbon was achieved under the experimental conditions of an activation temperature of 700 °C, activation time of 2 h, and impregnation ratio of 1:1. The activated carbon prepared under this experimental condition was named AC-R.

Figure 4 shows the nitrogen adsorption-desorption isotherm of AC-R. It can be seen that when $P/P_0 < 0.19$, AC-R exhibited monolayer adsorption at this stage, and the adsorption of nitrogen by AC-R increased with the increase of P/P_0. When $P/P_0 > 0.19$, AC-R began to exhibit multilayer adsorption, and the rate of adsorption of nitrogen by AC-R began to slow down; when $P/P_0 = 0.43$, the AC-R underwent nitrogen desorption; when $0.37 < P/P_0 < 0.97$, the adsorption-desorption isotherms of AC-R did not overlap, and according to the calculation, the average difference between the nitrogen adsorption value and the desorption value of AC-R in the interval was 23. This shows that the difference in the pore size of AC-R was large.

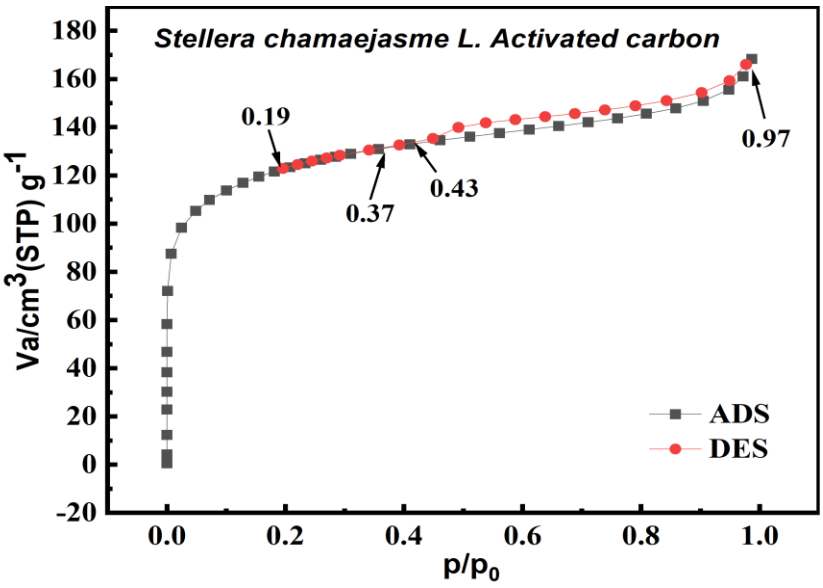

Fig. 4. The AC-R nitrogen adsorption-desorption isotherm

Figure 5 shows the pore size distribution of AC-R. It can be seen that the pore size values of AC-R are distributed at 0.5 to 3.1 nm; the dominant pore size is 0.945 nm, and the average pore size is 2.43 nm. Thus, AC-R was classed as mesoporous activated carbon.

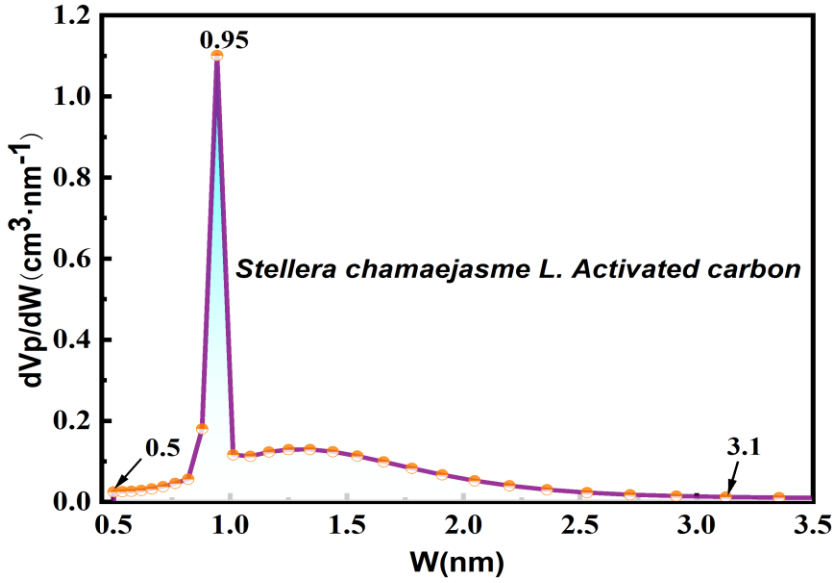

Fig. 5. The AC-R pore size distribution map

Table 1 shows the data comparison table between AC-R and related studies. The specific surface area of the activated carbon prepared by Zhang *et al.* (2024) using lignin as the raw material and rubidium chloride as the activator was 433 m^2/g with an average pore size of 2.02 nm (Table 1). This can be seen from the data comparison in Table 1. The *S. chamaejasme* Linn activated carbon prepared in this study had high specific surface area and pore volume.

Table 1. Comparison Table of Data from AC-R and Related Studies

Activator	Raw material	Activation Temp (°C)	Activation Time (h)	Impreg-nation Ratio	Specific Surface Area (m^2/g)	Pore Volume (cm^3/g)	Ref.
Rubidium chloride	*S. chamaejasme* L.	700	2	1:1	877.02	0.26	This study
Rubidium chloride	Lignin	600	2	5:1	433.32	0.21	Zhang *et al.* 2024

Figure 6 shows the scanning electron microscope (SEM) images of *Stellera chamaejasme* raw material (6a), *S. chamaejasme* charcoal (6b), and AC-R (6c-6d). As shown in Fig. 6, no obvious void structure was apparent on the surface of the *S. chamaejasme* raw material (6a); the surface of the inactivated *S. chamaejasme* charcoal was similar to that of the *S. chamaejasme* raw material (6b); and the activated *S. chamaejasme* Linn activated charcoal surface appeared to have an obvious void structure after the activation (6c, 6d). The activation mechanism of rubidium chloride has not yet been clarified, so it is not possible at this point to determine the cause of void formation on the AC-R surface. This study provides theoretical support for subsequent studies on the activation mechanism of rubidium chloride.

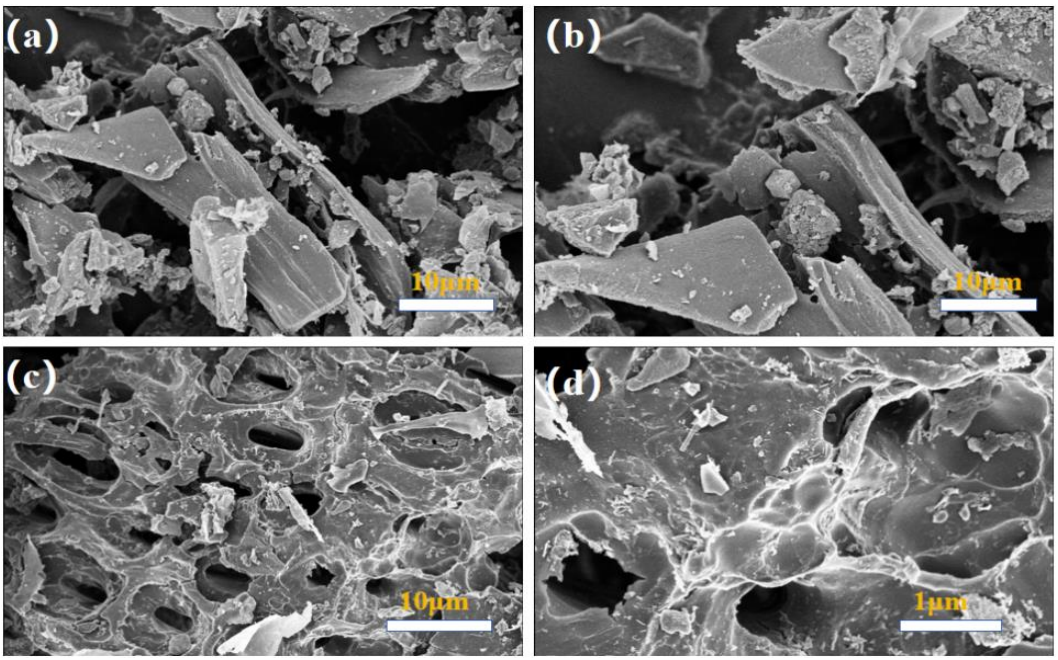

Fig. 6. Scanning electron microscope images of *S. chamaejasme* at 10 μm (a), SEM images of *S. chamaejasme* charcoal at 10 μm (b), SEM images of AC-R at 10 μm (c) and 1 μm (d)

Figure 7 shows the XRD analysis pattern of AC-R. As shown, there were obvious characteristic peaks in the interval of 2θ of 15 to 32.5°, which shows a certain crystal structure within the AC-R. There were irregular diffraction peaks at 2θ = 26.85° and 2θ = 29.4°. The miscellaneous peaks were fitted and compared with the standard PDF card, which shows that at 2θ = 29.4° is the characteristic peak eigen-peak of $CaCO_3$, and 2θ = 26.85° is the characteristic peak of SiO_2. The crucible powder remaining in the activated carbon led to the generation of the characteristic peak of SiO_2; when extracting the crude fiber of *S. chamaejasme*, $Ca(OH)_2$ remaining in the activated carbon reacted with CO_2 and eventually formed $CaCO_3$ leading to the generation of the characteristic peak.

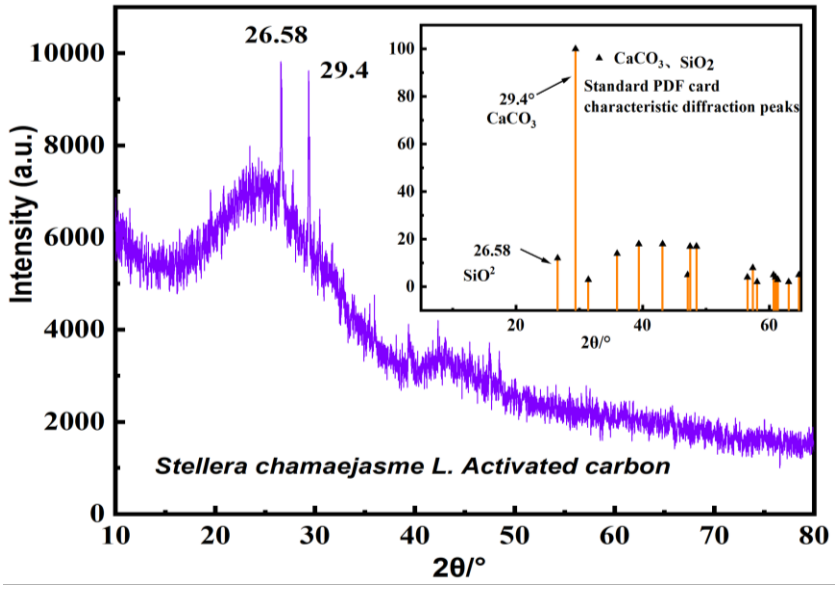

Fig. 7. The AC-R XRD diffraction pattern

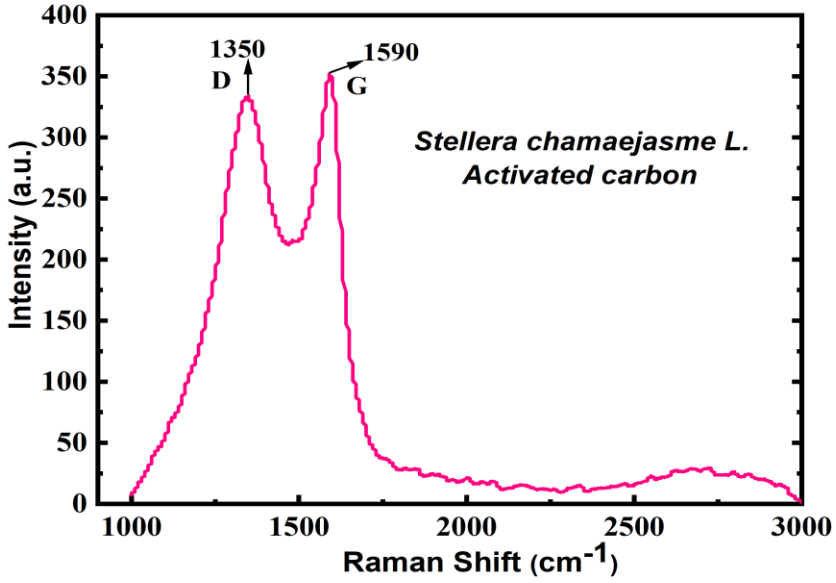

Fig. 8. The AC-R Raman spectrum data map

The Raman spectra of AC-R are shown in Fig. 8, from which the D-peak peak value of AC-R was 1350 cm^{-1} and the G-peak peak value was 1590 cm^{-1}. The D peak represents

the irregular vibration peak of the carbon atom, which belongs to the sp^3 vibration peak, and the G peak represents the regular vibration peak of the carbon atom, which belongs to the sp^2 vibration peak. The degree of graphitization of activated carbon can usually be characterized by I_D/I_G, and when $I_D/I_G \geq 0.8$, the activated carbon has a certain degree of graphitization. The larger the I_D/I_G, the higher the degree of graphitization of the activated carbon, and the I_D/I_G of AC-R = 0.85, which shows that AC-R has a certain degree of graphitization from the numerical analysis.

Figure 9 shows the surface functional group analysis of *S. chamaejasme* raw material, AC-R. Observation of the infrared curve of *S. chamaejasme* in Fig. 9a shows that *S. chamaejasme* exhibited obvious absorbance peaks of aromatic compounds and C-O groups in the infrared wavelength interval of 500 to 1250 cm^{-1} (Zhang *et al.* 2024); observation of the infrared curve of AC-R in Fig. 9a include an absorbance peak generated by vibration of C-O groups at 1220 cm^{-1} for AC-R and an absorbance peak generated by vibration of C = C groups at 1590 cm^{-1} for AC-R (Zhang *et al. 2023*). A comparison of the two FT-IR curves in Fig. 9a shows that *S. chamaejasme* lost many functional groups of alcohols, esters, and aromatic compounds upon activation (Chen *et al.* 2015).

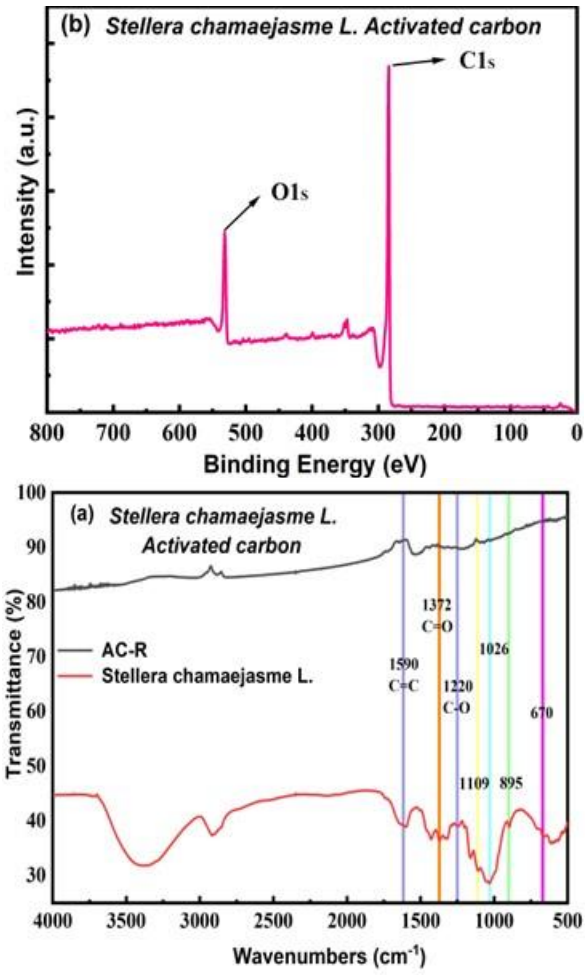

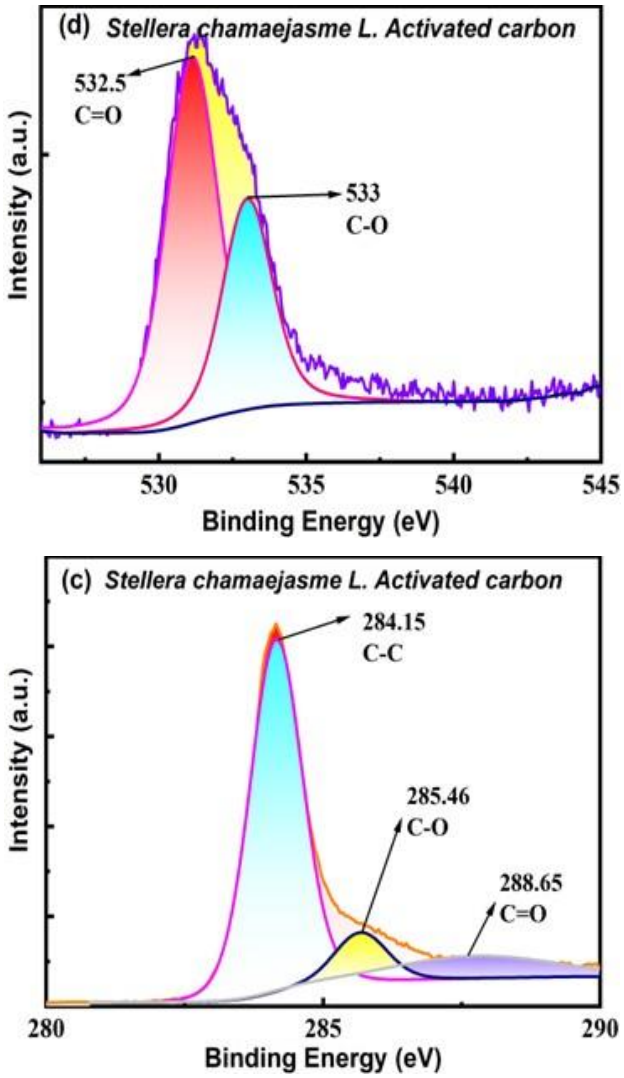

Fig. 9. FT-IR diagram of activated carbon AC-R (a), AC-R XPS scanning overview (b), AC-R XPS C1s scanning general view (c), AC-R XPS O1s scanning general view (d)

Figure 9b shows the total XPS scanning spectra of AC-R, Fig. 9c shows the fitted XPS scanning spectra of AC-R for carbon, and Fig. 9d shows the fitted XPS scanning spectra of AC-R for oxygen. Carbon and oxygen are most prominent in the scanning peaks of AC-R XPS (9b). At the binding energies of: 284.15 eV, 285.46 eV, and 288.65 eV, the corresponding functional groups are C-C, C-O, and C=O, respectively (9c) (Burg *et al. 2002*). At the binding energies of 532.5 eV and 533 eV, the corresponding functional groups are C=O and C-O (9d) (Zhang *et al.* 2024).

CONCLUSIONS

1. The ash content of *S. chamaejasme* was 3.12% ± 0.15%; thus, *S. chamaejasme* can be classified as a low ash material.
2. *S. chamaejasme* was used as the raw material for the preparation of activated carbon, rubidium chloride was used as the chemical activator, and the *S. chamaejasme*

mesoporous activated carbon was successfully prepared under the experimental conditions of an activation temperature of 700 ℃, activation time of 2 h, and impregnation ratio of 1:1.

3. The carbon yield of *S. chamaejasme* mesoporous activated carbon reached 13.55% ± 0.41%, with a dominant pore size of 0.945 nm, an average pore size of 2.43 nm, a pore volume of 0.26 cm^3/g, and a specific surface area of 877 m^2/g, with adsorption of iodine reaching 891 mg/g, and of methylene blue reaching 257 mg/g.
4. The *S. chamaejasme* mesoporous activated carbon exhibited a certain degree of graphitization and microcrystalline structure, and the surface functional groups were mainly carbon-containing and oxygen-containing functional groups.

ACKNOWLEDGMENTS

This research project was supported by the Qinghai Province Key R&D and Transformation Programme (2022-QY-210).

REFERENCES CITED

Ahmed, Z. T., Hand, D. W., Sutter, L. L., and Watkins, M. K. (2014). "Fly ash iodine number for measuring adsorption capacity of coal fly ash," *ACI Materials Journal* 111(4), 383-390. DOI: 10.14359/51686582

Buah, W. K., Darmey, J., and Osei, F. (2019). "Effects of maturity of coconut shells on gold adsorption efficiencies of derived activated carbons," *Ghana Mining Journal* 19(2), 50-54. DOI: 10.4314/gm.v19i2.7

Burg, P., Fydrych, P., Cagniant, D., Nanse, G., Bimer, J., and Jankowska, A. (2002). "The characterization of nitrogen-enriched activated carbons by IR, XPS and LSER methods," *Carbo*n 40, 1521-1531. DOI: 10.1016/s0008-6223(02)00004-0

Chen, C. C., Li, Y. L., Zhang, Z. Q., and Liu, X. J. (2024). "Study on dissolution crystallization for extraction of potassium and separation of magnesium and lithium from salt lake brine," *Inorganic Chemicals Industry* 56, 34-39. DOI: 10.19964/j.issn.1006-4990.2023-0420

Chen, J., Yuan, C. D., Li, H. C., Zhang, L. J., and Xu, G. Y. (2015). "Preparation and characterization of activated carbon from Wolf root," *Journal of Chemical Engineering* 29(05), 1161-1166.

Columba, A., Berruti, F., and Briens, C. (2022). "Model for the physical activation of biochar to activated carbon," *Journal of Analytical and Applied Pyrolysis* 168, article 105769. DOI: 10.1016/j.jaap.2022.105769

Doczekalska, B., Bartkowiak, M., Łopatka, H., and Zborowska, M. (2022). "Activated carbon prepared from corn biomass by chemical activation with potassium hydroxide," *BioResources* 17(1), 1794-1804. DOI: 10.15376/biores.17.1.1794-1804

Du, G. W. (2014). "New thoughts of comprehensive development and utilization of salt lake resources in Qinghai Province," *Acta Geologica Sinica* 88(s1), article 417. DOI: 10.1111/1755-6724.12280_1

Jo, B-G., Bong, S-K., Jegal, J., Kim, S-N., and Yang, M. H. (2020). "Antiallergic effects of phenolic compounds isolated from *Stellera chamaejasme* on RBL-2H3 cells,"

Natural Product Commun. 15(7), article 17. DOI: 10.1177/1934578X20942352

Kim, S., Lee, S-E., Baek, S-H., Choi, U., and Bae, H-J. (2023). "Preparation of activated carbon from Korean anthracite: Simultaneous control of ash reduction and pore development," *Processes* 11(10), article 2877. DOI: 10.3390/pr11102877

Kunusa, W. R., Iyabu, H., and Abdullah, R. (2021). "FTIR, SEM and XRD analysis of activated carbon from sago wastes using acid modification," *Journal of Physics: Conference Series* 1968(1), article 12014. DOI: 10.1088/1742-6596/1968/1/012014

Li, H. C., Sun, H. Z., and Xu, G. Y. (2009). "Tibetan paper from *Stellera chamaejasme* and reclamation of poisonous plants in grassland," *Journal of Xizang University (Natural Science Edition)* 24(1), 1-4. DOI: 10.16249/j.cnki.54-1034/c.2009.01.005

Ren, X., Shu, X., Geng, W., Li, P., and Xu, Y. (2024). "A study on the adsorption of methylene blue by acid-modified coal measures kaolin," *Processes* 12(4), article 773. DOI: 10.3390/pr12040773

Wang, J., Liu, T. L., Huang, Q-X., Ma, Z-Y., Chi, Y., and Yan, J-H. (2017). "Production and characterization of high quality activated carbon from oily sludge," *Fuel Processing Technology* 162, 13-19. DOI:10.1016/j.fuproc.2017.03.017

Zhang, C., Li, H., and Du, B. X. (2023). "Preparation and characterization of cellulose-based activated carbon by cesium chloride chemical method," *BioResources* 19(1), 1259-1304. DOI: 10.15376/biores.19.1.1295-1304

Zhang, C., Li, H., and Du, B. (2024). "Preparation and characterization of lignin-based activated carbon by rubidium chloride chemical method," *Chemistry Select* 9(20), article e202401258. DOI:10.1002/slct.202401258

Zhang, H., Xing, L., Liang, H., Ren, J., Ding, W., Wang, Q., Geng, Z., and Xu, C. (2022). "Efficient removal of Remazol Brilliant Blue R from water by a cellulose-based activated carbon," *International Journal of Biological Macromolecules* 207, 254-262. DOI: 10.1016/j.ijbiomac.2022.02.174

Zhao, L., Zhang, Y., Yin, Q., Chen, G., Li, W., and Li, N. (2023). "Research progress on the toxicity of toxic traditional herbals from Thymelaeaceae," *Journal of Ethnopharmacology* 322, article 117594. DOI:10.1016/j.jep.2023.117594

Article submitted: July 17, 2024; Peer review completed: August 7, 2024; Revised version received: August 14, 2024; Accepted: September 1, 2024; Published: September 13, 2024.
DOI: 10.15376/biores.19.4.8312-8323